Analytical Coupled Modeling and Model Validation of Hydraulic On/Off Valves

John Mahrenholz
e-mail: jmahrenh@purdue.edu

John Lumkes, Jr.
e-mail: lumkes@purdue.edu

Department of Agricultural and Biological Engineering,
Purdue University,
West Lafayette, IN 47907

The goal of this paper is to describe a method for modeling high speed on/off valves. This model focuses on the nonlinearities of the electromagnetic, fluidic, and mechanical domains, specifically within solenoid driven poppet style valves. By including these nonlinearities, the model accurately predicts valve transition time for different driving voltages and valve strokes. The model also predicts fluid transients such as pressure ripple. Unique attributes of the model are the inclusion of the effect of eddy currents and fringing while still being fully coupled with the fluid and mechanical domains. A prototype was constructed and used to experimentally validate the model. By developing accurate lumped parameter models, valve dynamics can be applied to hydraulic systems to accurately capture their dynamics. [DOI: 10.1115/1.4000072]

Keywords: hydraulic valve, analytical model, electromagnetics, poppet, model validation

1 Introduction

High speed, on/off valves are an enabling technology for exciting new advances in fluid power. They provide the fast switching characteristics necessary for hydraulic fluid pulse width modulation (PWM), active dampening systems, fuel injectors, and many other systems [1–6]. In some cases, high speed valves open up new system architectures [7]. This paper presents a model to accurately simulate these valves.

Because system dynamics are often dominated by high speed on/off valves, models must be very accurate. These systems often incorporate many of these valves amplifying computation time. Numerical models do a very good job of capturing valve performance, but often times they are too computationally expensive for use in systems level modeling. To reduce simulation time, a lumped parameter model was developed. Because the transition time is so important to these switching concepts, a highly coupled model that accurately describes the nonlinearities in the fluidic, electromagnetic, and mechanical domains is necessary. Lumped parameter models for valves were described in earlier works [8–10]. The new work presented in this paper is the addition of nonlinearities in the electromagnetic coupled models with traditional lumped parameters representing the fluidic domains. The electromagnetic nonlinearities include fringing and eddy currents. Fluid domain models include flows and forces for both the poppet sealing surface and spool sliding surface.

The model developed in this work has the ability to adapt to different geometries based on a series of fundamental equations. These equations are not dependent on empirical data for modeling accuracy. Because of this, the model can be used to study valve tradeoffs without production of numerous prototypes.

To verify the model, a prototype valve was constructed, as shown in Fig. 1. This prototype could be shimmed to develop different poppet strokes to test the model. Ports for high speed piezoresistive pressure transducers that could accurately capture pressure transients were included within the valve geometry.

Both dry and fluid testing was performed to verify the model. Dry testing was done to capture the transition profile of the poppet. A high speed noncontact laser was used to capture these transition profiles. Fluid testing was used to verify that the model accurately captures the effect of flow forces on the transition time and fluid dynamics of the system.

2 Valve Prototype

For the prototype, a three-port two-position valve was chosen, as this allowed a pressure balanced poppet design.

When Electromagnet A (EM_A, Fig. 1) is in the ON state, the steel force ring transmits the electromagnetic force to the poppet. This causes the poppet to shift, opening the flow path between Port A and Port C. Conversely, by activating EM_B, the poppet will shift closing the path between Ports A and C, and opening the path between Port A and B. The housing and the poppet were made from billet aluminum to ensure they would have no effect on the performance of the electromagnetics. Specifically, the housing was made out of 6061-T6 billet aluminum to ensure it would deform before the harder 7072 billet aluminum poppet. The electromagnetic cups and steel force ring were built using AISI 1020 mild steel with copper windings. Three pressure transducer ports

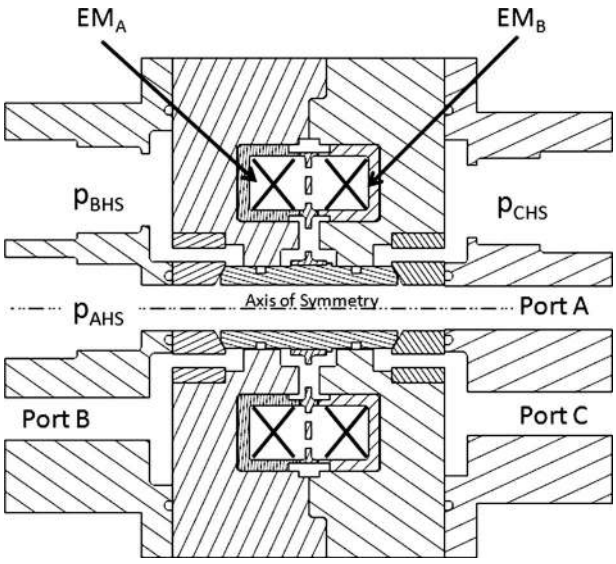

Fig. 1 Prototype description

Contributed by the Dynamic Systems Division of ASME for publication in the JOURNAL OF DYNAMIC SYSTEMS, MEASUREMENT, AND CONTROL. Manuscript received December 4, 2008; final manuscript received July 22, 2009; published online December 3, 2009. Assoc. Editor: J. Karl Hdrick.

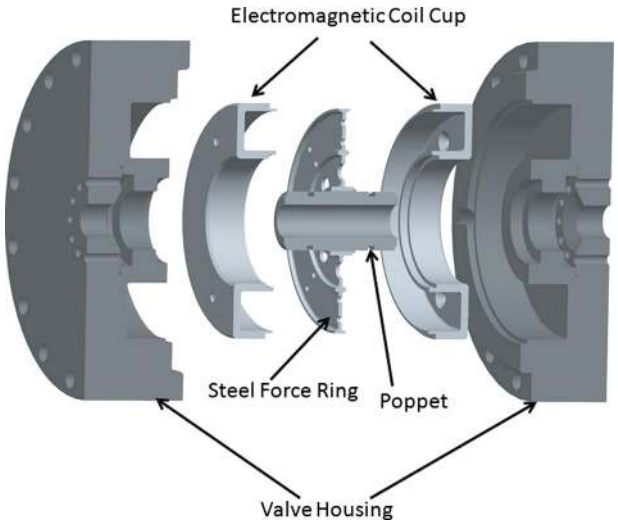

Fig. 2 Valve cutaway

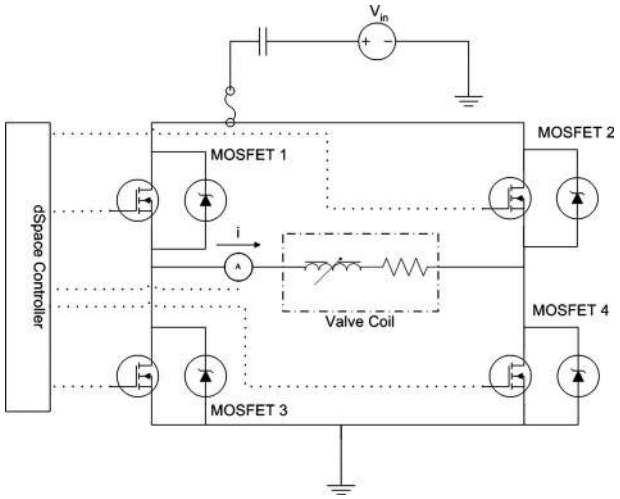

Fig. 4 Driving circuitry

were integrated into the valve housing (signified by p_{HS} in Fig. 1). To adjust the stroke of the valve, shims could be placed between the middle sections of the housing, as seen in Fig. 2.

3 Modeling

3.1 Model Description. The model of the valve includes five components representing three domains. Each component and domain is highly coupled with the others. The electromagnetic model focuses on the relationship of input voltage and output force. This model requires the position and velocity of the valve poppet. The fluid dynamics model describes the forces on the poppet and the leakage from the spool surface. It requires valve position and velocity, as well as inlet flow and outlet pressure. The dynamic motion model represents the mechanical domain. It integrates forces from the other models, and outputs position and velocity of the poppet. The pump model develops fluid flow, and simulates a relief valve to limit pressure spikes. The load model represents a load on the system. It produces an outlet pressure based on system flow. The overall method for modeling is time based. The fluid dynamics and electromagnetic models are designed to be calculated concurrently at each time step. Their results are fed into the dynamic motion model, which then feeds back the corresponding velocities and position at the next time step. Figure 3 shows how each submodel integrates into the overall system model.

3.2 Electromagnetics. The electromagnetic model takes as input the transistor state, voltage, poppet position, and poppet velocity. The output of the model includes electromagnetic force and coil current. Fringing effects and eddy currents have a large effect on valve transition time, so they are accounted for in the model. For simplicity and reduced computational time, the model assumes that magnetic saturation and hysteresis can be ignored. This assumption is reasonable for strictly on/off valves, as steady state force has little effect on valve dynamics, with the exception of cases involving low switching voltages. In these cases, steady state force is reached before the valve is fully switched. Because the majority of the electromagnetic cups are relatively thick, leading to low flux densities in most of the core, leakage flux can also be ignored. The first step in modeling the electromagnets is to determine voltage seen by the coil from the driving circuits.

Figure 4 shows the circuit used to control one coil within the valve. This circuit consists of an H-bridge using four MOSFETs with integrated Zener diodes. The MOSFETs are driven using an IRS2117 single channel MOSFET driver (schematic shown in Fig. 5) that maintains the gate voltage, 10 V above the floating source voltage.

For this model, a simple driving method is assumed. In the on state, MOSFETs 1 and 4 are activated. Current then flows from the voltage source through the coil left to right and finally to ground. In the OFF state, all four MOSFETs are deactivated. Once the MOSFETs are deactivated, the inductance of the coil causes electrons to be pulled through the diode of MOSFET 3, and pushed through the diode of MOSFET 2. Because this action causes a voltage rise, a decay voltage equal to the source voltage (V_{in}) is imposed upon the coil.

Therefore, in the ON state, the system voltage (V_{sys}) is equal to the input voltage, assuming no voltage drop across the MOSFET. In the off state, the voltage is then the decay voltage. Since the turn on and turn off time of an IRF640 MOSFET is less the 100 ns, the dynamics of the MOSFETs can be neglected [11]

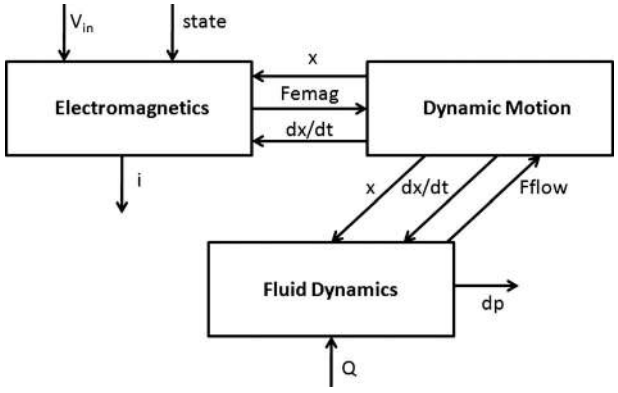

Fig. 3 Model dynamics

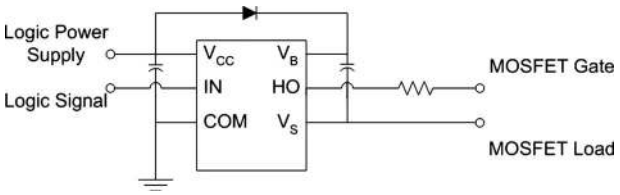

Fig. 5 IRS2117 MOSFET driver schematic

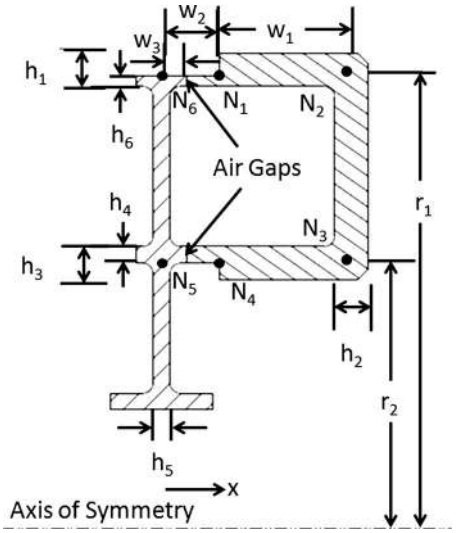

Fig. 6 Node locations and electromagnetic geometry

$$V_{\text{sys}} = \begin{cases} V_{\text{in}} & \text{for state = on} \\ V_{\text{decay}} & \text{for state = off} \end{cases} \tag{1}$$

The decay voltage is modeled as

$$V_{\text{decay}} = \begin{cases} -V_{\text{in}} & \text{for } i > 0 \\ 0 & \text{for } i \le 0 \end{cases} \tag{2}$$

The voltage drop across the coils is represented by three components: the voltage drop due to coil resistance (Ω), change in inductance (dL/dt), and change in current (di/dt) [12]. The sum of these components is equal to the system voltage

$$V_{\text{sys}} = i\Omega + i\left(\frac{dL}{dt}\right) + L(x)\left(\frac{di}{dt}\right) \tag{3}$$

Rearranging terms yields a solution for current flowing through the coil as

$$i = \int \frac{V_{\text{sys}} - i\Omega - i\left(\frac{dL}{dt}\right)}{L(x)} dt \tag{4}$$

Equation (4) shows that the current rises and decays faster as V_{in} (and therefore V_{sys}) increases.

The total inductance of the coils is defined by the number of wire turns (N) squared, divided by the total reluctance ($R(x)$) of the flux path [13]

$$L(x) = \frac{N^2}{R(x)} \tag{5}$$

Figure 6 shows the electromagnetic geometry for one coil used within the prototype. The geometry is broken into six segments, which link the six nodes shown in the figure. The following equations describe how the total reluctance $R(x)$ is calculated from the geometry.

The permeability of the steel magnet is defined by the relative permeability (μ_R) and the magnetic constant (μ_0) [13]

$$\mu = \mu_0(\mu_R) \tag{6}$$

The reluctance of an axial section of the electromagnetic core can be found using the area (A) and length (L) of the section with the previously calculated permeability [13]

$$R_{\text{Axial}} = \frac{L}{\mu A} \tag{7}$$

Since a thin annular cross section is used, the area can be modeled as the circumference of the center line of the section, multiplied by the thickness as

$$R_{\text{Axial}} = \frac{w}{\mu(2\pi rh)} \tag{8}$$

Substituting for the section linking nodes 1 and 2 (Secs. 1 and 2), and using the dimensions shown in Fig. 6, yields

$$R_{12} = \frac{w_1}{\mu(2\pi r_1 h_1)} \tag{9}$$

The cross sectional area changes as a function of length for the radial sections, which requires additional computations. The formula for reluctance of a radial section is defined as [14]

$$R_{\text{Radial}} = \int_{r_i}^{r_o} \frac{1}{2\pi h\mu r} dr = \frac{1}{2\pi h\mu} \ln\left(\frac{r_o}{r_i}\right) \tag{10}$$

Substituting known quantities for Secs. 2 and 3 yields

$$R_{23} = \frac{\ln\left(\frac{r_1}{r_2}\right)}{2\pi\mu(h_2)} \tag{11}$$

By using Eqs. (8) and (10), reluctance for the remaining sections can be found as follows:

$$R_{34} = \frac{w_1}{\mu(2\pi r_2 h_3)} \tag{12}$$

$$R_{45} = \frac{w_2}{\mu(2\pi r_2 h_4)} \tag{13}$$

$$R_{56} = \frac{\ln\left(\frac{r_2}{r_1}\right)}{2\pi\mu(h_5)} \tag{14}$$

$$R_{61} = \frac{w_2}{\mu(2\pi r_1 h_6)} \tag{15}$$

The reluctance at zero air gap is defined as the sum of the reluctances of the individual sections as

$$R_0 = R_{12} + R_{23} + R_{34} + R_{45} + R_{56} + R_{61} \tag{16}$$

The total air gap x_{act} is defined as the sum of the simulation position ($x=0$ when poppet is centered), electromagnetic minimum gap (x_0), and half of the stroke ($\Delta x_{\max}$).

For coil A

$$x_{\text{act}} = x + x_0 + \frac{\Delta x_{\max}}{2} \tag{17}$$

For coil B

$$x_{\text{act}} = -x + x_0 + \frac{\Delta x_{\max}}{2} \tag{18}$$

Using the actual air gap, the reluctance including fringing effects can be modeled as [15]

$$R_{\text{AG1}} = \frac{1}{\mu_0 2\pi r_1 \left[\frac{h_6}{x_{\text{act}}} + \frac{2}{\pi}\left(1 + \ln\frac{\pi w_3}{4x_{\text{act}}}\right)\right]} \tag{19}$$

$$R_{AG2} = \frac{1}{\mu_0 2\pi r_2 \left[\frac{h_4}{x_{act}} + \frac{2}{\pi}\left(1 + \ln\frac{\pi w_3}{4x_{act}}\right)\right]} \tag{20}$$

The total reluctance including air gap can be found by adding each air gap in the series with the reluctance at zero air gap

$$R(x) = R_0 + R_{AG1} + R_{AG2} \tag{21}$$

The total reluctance can then be used in combination with the number of coil turns to determine the inductance of the coil with respect to x using Eq. (5). The total inductance can then be substituted into Eq. (4). The final component necessary to determine the current flowing through the coil is the derivative of inductance with respect to time, which is analytically found in the following section of equations.

First, the derivative of the reluctance with respect to position for each air gap is found by taking the derivatives of Eqs. (19) and (20) as

$$\frac{dR_{AG1}(x)}{dx} = \mu_0 2\pi r_1 \left[\frac{h_6}{x_{act}^2} + \frac{2}{\pi x_{act}}\right]\frac{dx_{act}}{dx} R_{AG1}^2 \tag{22}$$

$$\frac{dR_{AG2}(x)}{dx} = \mu_0 2\pi r_2 \left[\frac{h_4}{x_{act}^2} + \frac{2}{\pi x_{act}}\right]\frac{dx_{act}}{dx} R_{AG2}^2 \tag{23}$$

where dx_{act}/dx is the sign of the x term in the definition of x_{act}, originally defined in Eqs. (17) and (18).

Because the reluctance at zero air gap (R_0) is constant, the change in total reluctance with respect to x is the sum of the derivative of the two air gaps

$$\frac{dR(x)}{dx} = \frac{dR_{AG1}(x)}{dx} + \frac{dR_{AG2}(x)}{dx} \tag{24}$$

The derivative of inductance can then be modeled as

$$\frac{dL(x)}{dx} = -\frac{N^2 \frac{dR(x)}{dx}}{R(x)^2} \tag{25}$$

The change in inductance over time is then defined as the derivative of inductance with respect to x, multiplied by the velocity of the poppet [12] (Note: This is true because the inductance at a specific poppet position does not change over time)

$$\frac{dL}{dt} = \frac{dL(x)}{dx}\left(\frac{dx}{dt}\right) \tag{26}$$

The result of Eq. (26) is fed back into Eq. (4), along with the current of the previous time step, to determine the new current flowing through the coil. This process is repeated until the end of the simulation.

The instantaneous flux can then be defined by the inductance and current flowing through the coil [13]

$$\phi_{inst} = i(L(x)) \tag{27}$$

Eddy currents are modeled in the Laplace domain using a first order lag of the instantaneous flux as

$$\frac{\phi(s)}{\phi_{inst}(s)} = \frac{1}{\tau_{ec}s + 1} \tag{28}$$

The time constant for the outer edge of the steel core is defined as [16]

$$\tau_{ec\_oe} = 4\sigma\mu\left(\frac{h}{\pi}\right)^2 \tag{29}$$

Since the time constant at the inside edge of the coil is essentially zero, the overall time constant for the core is assumed to be the average

$$\tau_{ec} = \frac{\tau_{ec\_oe}}{2} = 2\sigma\mu\left(\frac{h}{\pi}\right)^2 \tag{30}$$

Since the restricting area of the inside and outside air gaps is the same, the model uses the average thickness of the two air gaps

$$\tau_{ec} = 2\sigma\mu\left(\frac{h_4 + h_6}{2\pi}\right)^2 \tag{31}$$

The force of the electromagnet can then be defined as the square of the flux, multiplied by the derivative of the reluctance with respect to x. Note that this force is defined in the negative x-direction for electromagnet A, and in the positive x-direction for electromagnet B [13]

$$F_{emag} = \frac{1}{2}\phi^2 \frac{dR(x)}{dx} \tag{32}$$

3.3 Fluid Dynamics. The fluidic model simulates pressure drop and fluid force on the poppet from inputs of fluid flow, poppet position, and poppet velocity. The model uses turbulent or laminar models for the orifice, depending on the Reynolds number. It determines leakage into the coil using a Poiseuille flow leakage model (pressure driven flow). Because the valve motion is oscillatory, leakage due to Couette flow (velocity driven) is considered negligible. Flow forces are developed using Navier–Stokes and fluid momentum terms. Frictional forces are also developed in this model, using both Couette and Poiseuille sliding friction models.

The orifice area of the valve is a function of the position and circumference of the poppet.

For orifice connecting ports A and B in Fig. 1 (orifice A-B)

$$A = 2\pi r_{valve}\left(x + \frac{\Delta x_{max}}{2}\right) \tag{33}$$

For orifice A-C

$$A = 2\pi r_{valve}\left(-x + \frac{\Delta x_{max}}{2}\right) \tag{34}$$

The wetted perimeter of the orifice is equal to two times the circumference of the sealing edge

$$S = 4\pi r_{valve} \tag{35}$$

The pressure drop across the orifice is simply defined as the difference between the pressure of the two sides.

For orifice A-B

$$\Delta p_{AB} = p_A - p_B \tag{36}$$

For orifice A-C

$$\Delta p_{AC} = p_A - p_C \tag{37}$$

The hydraulic diameter of each orifice is defined as [9]

$$D_H = \frac{4A}{S} \tag{38}$$

Rearranging terms, the hydraulic diameter is equal to twice the valve opening.

For orifice A-B

$$D_H = x + \frac{\Delta x_{max}}{2} \tag{39}$$

For orifice A-C

$$D_H = -x + \frac{\Delta x_{max}}{2} \tag{40}$$

The Reynolds number can then be computed using the following equation [9]:

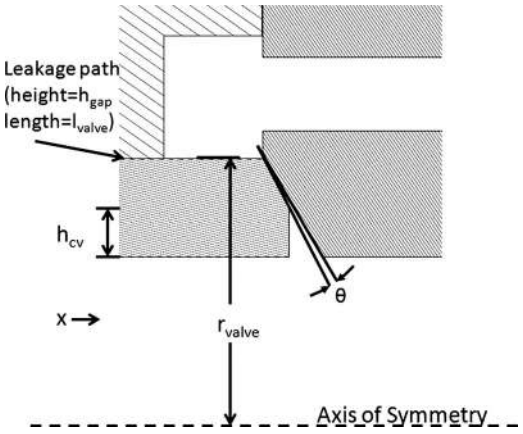

Fig. 7 Flow passage dimensions

$$\mathrm{Re} = \frac{QD_H}{Av} \tag{41}$$

Two different flow conditions exist for the orifice, turbulent, and laminar. The cutoff between these two conditions is defined by the critical Reynolds number [9]

$$Q_{\text{orifice}} = \begin{cases} C_D A \ \text{sign}(\Delta p)\sqrt{\frac{2}{\rho}|\Delta p|} & \text{for } \mathrm{Re} \geq \mathrm{Re}_{\text{cr}} \\ 2C_{DL}A\frac{D_H}{v\rho}\Delta p & \text{for } \mathrm{Re} < \mathrm{Re}_{\text{cr}} \end{cases} \tag{42}$$

The leakage coefficient for Poiseuille flow through the spool sealing surface can then be defined as [17]

$$k_{\text{leakage\_press}} = \frac{\pi}{(6\mu_{\text{fl}})}\frac{1}{l_{\text{valve}}} r_{\text{valve}} h_{\text{valve}}^3 \tag{43}$$

Since the coils are kept at tank pressure, simply multiplying the pressure drop from the outlet port to the tank by the leakage coefficient gives the leakage flow [17]. This leakage path is shown in Fig. 7.

For Side B

$$Q_{\text{leakage}} = (p_B - p_T)k_{\text{leakage\_press}} \tag{44}$$

For Side C

$$Q_{\text{leakage}} = (p_C - p_T)k_{\text{leakage\_press}} \tag{45}$$

The total flow out of the port is then the difference in the orifice flow and the leakage flow

$$Q_{\text{port}} = Q_{\text{orifice}} - Q_{\text{leakage}} \tag{46}$$

Since terms will eventually be divided by $|\Delta p|$, a small offset was added to ensure model fidelity during momentary transition times

$$|\Delta p|_{\text{offset}} = |\Delta p| + 0.1 \ \text{Pa} \tag{47}$$

The valve coefficient β is a function of the discharge coefficient and the fluid density [9]

$$\beta = C_D\sqrt{\frac{2}{\rho}|\Delta p|_{\text{offset}}} \tag{48}$$

The flow gain can then be defined using β, the radius of the valve, and the sealing angle of the poppet [9]

$$K_q = 2\pi r_{\text{valve}}\beta \sin(\theta) \tag{49}$$

The pressure flow gain is defined as [9]

$$K_c = \frac{2\pi r_{\text{valve}}\beta\Delta x_{\max}\sin(\theta)}{2|\Delta p|_{\text{offset}}} \tag{50}$$

The flow force gain can also be defined using the valve radius, discharge coefficient, and seat angle [9]

$$K_{fq} = 4\pi r_{\text{valve}} C_D^2 |\Delta p|_{\text{offset}} \sin(\theta)\cos(\theta) \tag{51}$$

Similarly, the pressure flow force gain is defined as [9]

$$K_{fc} = 4\pi r_{\text{valve}} C_D^2 \Delta x_{\max} \sin(\theta)\cos(\theta) \tag{52}$$

The flow force can then be found using the previous four gains. It should be noted that the first two terms are dynamic, and the last two are steady state. Also, this force is defined in the negative x-direction for orifice B, and in the positive x-direction for orifice C [9].

For Orifice B

$$F_{\text{Flow}B} = \rho h_{\text{cv}} K_q\left(\frac{dx}{dt}\right) + \rho h_{\text{cv}} K_c\left(\frac{d|\Delta p_{AB}|_{\text{offset}}}{dt}\right) + K_{fq}\left(x + \frac{\Delta x_{\max}}{2}\right) + K_{fc}|\Delta p_{AB}|_{\text{offset}} \tag{53}$$

For Orifice C

$$F_{\text{Flow}C} = \rho h_{\text{cv}} K_q\left(-\frac{dx}{dt}\right) + \rho h_{\text{cv}} K_c\left(\frac{d|\Delta p_{AC}|_{\text{offset}}}{dt}\right) + K_{fq}\left(-x + \frac{\Delta x_{\max}}{2}\right) + K_{fc}|\Delta p_{AC}|_{\text{offset}} \tag{54}$$

Forces also are exerted along the spool sealing surface.

The coefficient for the damping force due to velocity of the poppet (Couette flow force) can be defined using the length of the surface, the radius of the valve, the fluid viscosity, and the gap height [17]

$$b_{\text{valve\_}v0} = 2\pi l_{\text{valve}} r_{\text{valve}}\frac{\mu_{\text{fl}}}{h_{\text{gap}}} \tag{55}$$

The coefficient for force, due to pressure differential across the laminar gap (Poiseuille flow force), can be defined as well using the radius of the poppet and the gap height [17]

$$b_{\text{valve\_press}} = \pi h_{\text{gap}} r_{\text{valve}} \tag{56}$$

The total force from each sealing surface can be defined using coefficients calculated in Eqs. (55) and (56). As before, this force is defined in the negative x-direction for orifice B, and in the positive x-direction for orifice C [17]

For Side B

$$F_{\text{Fric}B} = -(p_B - p_T)b_{\text{valve\_press}} + \left(\frac{dx}{dt}\right)b_{\text{valve\_}v0} \tag{57}$$

For Side C

$$F_{\text{Fric}C} = -(p_C - p_T)b_{\text{valve\_press}} + \left(-\frac{dx}{dt}\right)b_{\text{valve\_}v0} \tag{58}$$

3.4 Dynamic Motion. The dynamic motion model develops poppet position and velocity from the output forces of the electromagnetic and fluidic models. The model assumes that the wall is composed of a stiff spring and damper system. The spring force is due to the intrusion of the poppet into the wall.

This intrusion is defined as

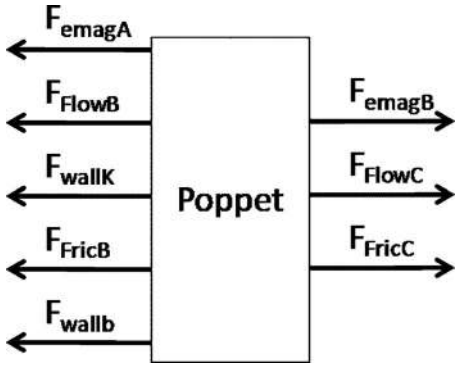

Fig. 8 Free-body diagram

$$x_{\text{wall}} = \begin{cases} x - \dfrac{\Delta x_{\max}}{2} & \text{for } x \geq \dfrac{\Delta x_{\max}}{2} \\ 0 & \text{for } -\dfrac{\Delta x_{\max}}{2} < x < \dfrac{\Delta x_{\max}}{2} \\ x + \dfrac{\Delta x_{\max}}{2} & \text{for } x \leq -\dfrac{\Delta x_{\max}}{2} \end{cases} \tag{59}$$

The spring force is then simply the intrusion multiplied by the wall spring coefficient [18]

$$F_{\text{wall}K} = k_{\text{wall}} x_{\text{wall}} \tag{60}$$

The damping force is assumed to increase further the poppet intrudes into the wall. This results from the ever increasing deformation of the surface. Leaving the wall, it is assumed that no dampening exists

$$F_{\text{wall}b} = \begin{cases} |x_{\text{wall}}| b_{\text{wall}} \dfrac{dx}{dt} & \text{for } \left[\dfrac{dx}{dt} \geq 0 \text{ and } x \geq \dfrac{\Delta x_{\max}}{2} \right] \text{ or } \left[\dfrac{dx}{dt} \leq 0 \text{ and } x \leq -\dfrac{\Delta x_{\max}}{2} \right] \\ 0 & \text{else} \end{cases} \tag{61}$$

Figure 8 shows the free body diagram for the poppet. The total force on the poppet is the sum of the electromagnetic, flow, friction, and wall forces derived in Eqs. (32), (53), (54), (57), (58), (60), and (61)

$$F_{\text{total}} = -F_{\text{emag}A} + F_{\text{emag}B} - F_{\text{Flow}B} + F_{\text{Flow}C} - F_{\text{Fric}B} + F_{\text{Fric}C} - F_{\text{wall}K} - F_{\text{wall}b} \tag{62}$$

The acceleration of the poppet is the resultant force divided by the mass [18] as

$$\frac{d^2x}{dt^2} = \frac{F_{\text{total}}}{m_{\text{poppet}}} \tag{63}$$

The velocity is the integral of acceleration [18] (initial velocity is assumed to be zero)

$$\frac{dx}{dt} = \int \frac{d^2x}{dt^2} dt \tag{64}$$

The position of the valve is the integral of velocity [18] (initial position is assumed to be $\Delta x_{\max}/2$ or the B port fully opened)

$$x = \int \frac{dx}{dt} dt \tag{65}$$

3.5 Pump. The pump consists of an ideal flow source and a relief valve. The cross sectional area of the relief valve is linearly dependent on the system pressure and the pressure setting

$$A_{\text{relief}} = \begin{cases} (p_A - p_T - p_{\text{setting}}) k_{\text{relief}} & \text{for } p_A - p_T - p_{\text{setting}} \geq 0 \\ 0 & \text{for } p_A - p_T - p_{\text{setting}} < 0 \end{cases} \tag{66}$$

The pressure drop across the valve is defined as the pressure difference between port A pressure and tank

$$\Delta p_{AT} = p_A - p_T \tag{67}$$

The flow through the relief valve is once again defined for both laminar and turbulent flows. The hydraulic diameter, laminar discharge coefficient, and Reynolds number are defined, as in the fluidic section [9]

$$Q_{\text{relief}} = \begin{cases} C_D A_{\text{relief}} \sin(\Delta p) \sqrt{\dfrac{2}{\rho} |\Delta p|} & \text{for } \text{Re} \geq \text{Re}_{\text{cr}} \\ 2 C_{DL} A_{\text{relief}} \dfrac{D_H}{\upsilon \rho} \Delta p & \text{for } \text{Re} < \text{Re}_{\text{cr}} \end{cases} \tag{68}$$

Fluid compressibility must also be taken into account in this system. The compressed fluid volume is based on the geometric fluid volume, the system pressure, and the bulk modulus of the fluid. The change in this volume over time is the compressibility flow [17]

$$V_{\text{comp}} = V_{\text{line}} - \frac{V_{\text{line}}}{E} p_{\text{line}} \tag{69}$$

$$Q_{\text{comp}} = \frac{dV_{\text{comp}}}{dt} \tag{70}$$

The total system flow is then the difference between the setting of the ideal flow source, the flow through the relief valve, and the compressibility flow

$$Q_{\text{sys}} = Q_{\text{setting}} - Q_{\text{relief}} - Q_{\text{comp}} \tag{71}$$

The system flow is then divided into orifice B and orifice C

$$Q_{AB} + Q_{AC} = Q_{\text{sys}} \tag{72}$$

3.6 Load. The load on the valve consists of a linear pressure drop and compressible volume. The compressible volume is defined the same way as the pump.

The flow through the linear pressure drop is defined as

$$Q_{\text{tank}} = Q_{\text{port}} - Q_{\text{comp}} \tag{73}$$

The pressure on the upstream side of the linear pressure drop is then

$$p = \frac{Q_{\text{tank}}}{k_{\text{load}}} - p_T \tag{74}$$

where k_{load} is the gain of the linear pressure drop. A list of the model parameters used, values, and units are given in Table 1.

4 Model Application to Other Geometries

The equations presented in the modeling section are designed to simulate one specific geometry: the prototype valve. However, the underlying equations can be used to solve for a multitude of different electromagnetic and poppet shapes.

In the electromagnetic domains, Eqs. (8) and (10) can be used to describe any axial radial segment material reluctance. By combining a series of these reluctances, a model of the required geometry is produced. Equation (19) can be used to model the reluctance of fixed and variable air gaps. Combining this with the material reluctance gives the parameters necessary for building a complete model of the electromagnet.

The fluid domains consist of two major components: the poppet flows and forces, and sliding spool surface flows and forces. The poppet model uses traditional valve gains, specifically, flow gain, pressure flow gain, flow force gain, and pressure flow force gain,

Table 1 Model parameters

Symbol	Value	Unit
C_D	Discharge coefficient	0.70
C_{DL}	Laminar discharge coefficient	0.040
E	Bulk modulus	8×10^{8} Pa
h_1	Thickness	2.50×10^{-3} m
h_2	Thickness	2.50×10^{-3} m
h_3	Thickness	2.50×10^{-3} m
h_4	Thickness	1.25×10^{-3} m
h_5	Thickness	1.25×10^{-3} m
h_6	Thickness	8.0×10^{-4} m
h_{gap}	Thickness	5.01×10^{-5} m
k_{wall}	Spring constant	7.0×10^{8} N/m
k_{load}	Linear pressure drop gain	$0-6\times10^{-6}$ L/(min Pa)
l_{valve}	Poppet sealing length	8.33×10^{-4} m
m_{poppet}	Poppet mass	0.045 kg
N	Number of coil turns	200
p_T	Tank pressure	0 Pa
$Q_{setting}$	System flow rate setting	0–40 L/min
r_1	Radial dimension	3.475×10^{-2} m
r_2	Radial dimension	2.025×10^{-2} m
r_{valve}	Radial dimension	9.00×10^{-3} m
Re_{cr}	Reynolds number	12
w_1	Axial dimension	8.63×10^{-3} m
w_2	Axial dimension	4.37×10^{-3} m
w_3	Axial dimension	1.59×10^{-3} m
x_0	Initial air gap	1.3×10^{-5} m
Δx_{max}	Valve stroke	$2.0\times10^{-4}-7.5\times10^{-4}$ m
V_{line}	Uncompressed line volume	0.12 L
V_{in}	Input voltage	10–180 V
θ	Valve angle	1.05 rad
μ_0	Permeability of free space	1.256×10^{-6} H/m
μ_{fl}	Dynamic viscosity	0.016 Pa s
μ_R	Relative permeability	600
υ	Kinematic viscosity	1.8×10^{-5} m^2/s
ρ	Fluid density	870 kg/m^3
Ω	Coil resistance	3.5 Ω
σ	Conductivity	6.0×10^{6} S/m

to determine flow forces. These gains can be determined for many different geometries in both spool and poppet style valves [9]. The sliding surface models are based off of gap flows, both Couette and Poiseuille. These models can be applied to any gap that has pressurized or sliding surfaces.

5 Model Application to Optimization

The purpose of this model is to optimize the valve for specific systems, depending on design requirements. To begin this process, design priorities must be established; these could include minimizing driving voltage, maximizing system efficiency, minimizing valve size, etc. Once these requirements are established and an initial geometry is determined, dimensions can be varied to optimize valve performance. Once the valve design has met design criteria, the optimization would end. Figure 9 shows a flow chart for one possible optimization routine.

6 Test Setup

The prototype valve was tested with and without oil, and the results were compared with the dynamic model simulation. The spool transition profile was measured during the dry testing, and the pressure and flow dynamics were measured during the fluid testing.

6.1 Dry Testing. The laser position measurement system shown in Fig. 10(*a*) was used to capture spool movement over time of the prototype valve shown in Fig. 10(*b*).

The laser sampling speed was set at 20 μs. At this speed, the laser had an accuracy of approximately 2 μm [19]. A plastic insert was added to the poppet to act as an optical target for the laser.

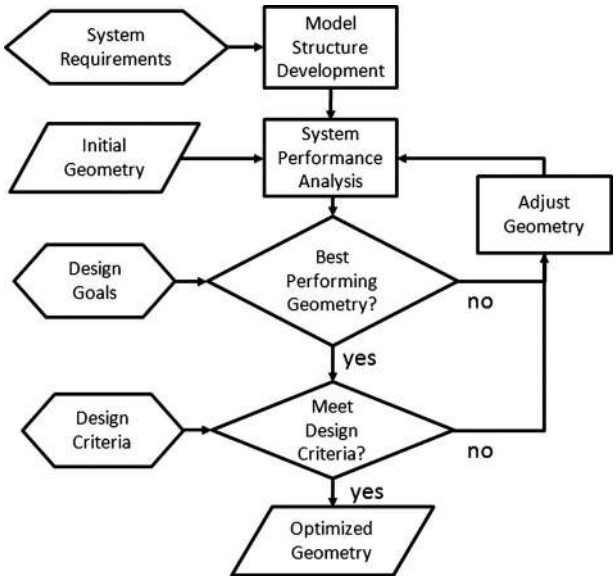

Fig. 9 Valve optimization flow chart

6.2 Fluid Testing. Fluid testing was done using a hydraulic test bench (hydraulic schematic of the test setup is shown in Fig. 11). The test bench supplies pressure and flow to the prototype valve.

Three variable orifices are used to control the inlet (orifice A) and outlet conditions of the valve (orifices B and C). High speed

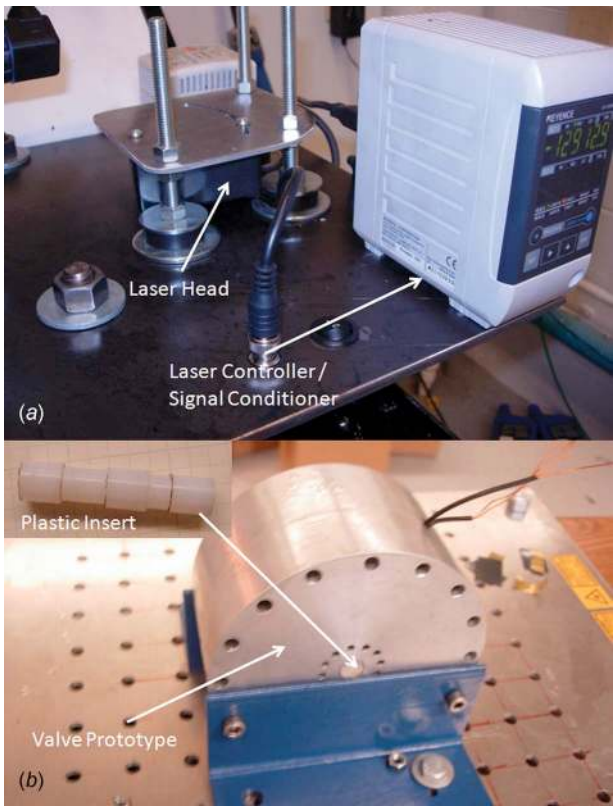

Fig. 10 (*a*) Laser test setup and (*b*) prototype

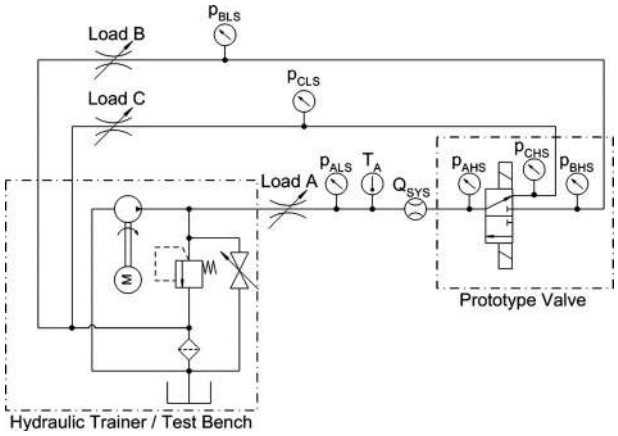

Fig. 11 Hydraulic test circuit

pressure transducers are integrated directly into the valve, as shown in Fig. 12 (labeled p_{*HS} in Fig. 11). These sensors capture pressure transients. Lower speed pressure transducers are used to determine steady state pressures (labeled p_{*LS} in Fig. 11). The valve was driven, and data was collected in both the fluid and dry testing with a dSpace DS1103 real-time control system, shown with external circuitry.

7 Test Results

7.1 Dry Testing. Normal, very high, and low voltages were used during testing of the valve to determine the accuracy of the model at peak currents ranging from 3 A to 30 A. Figure 13 shows simulated and test poppet position data versus time at 0.25 mm stroke.

The model works very well at medium voltages (40–100 V). At lower voltages, the model under predicts the transition time, due to the assumption of no saturation. Saturation of the steel core at flux densities higher than 2 T would limit the steady state force and result in improved accuracy at low voltages. At higher voltage, excess current drives down the eddy current time constant (τ_{ec}). This results in the model over predicting the transition time.

Figure 14 shows the valve transition profile for three different strokes at 60 V. The range of strokes corresponds to flow areas of 11–17.0 mm^2. The model accurately predicts the effect of different strokes.

7.2 Fluid Testing. Figure 15 shows the simulated and measured data outlet pressure of Port C for a 250 Hz wave. This

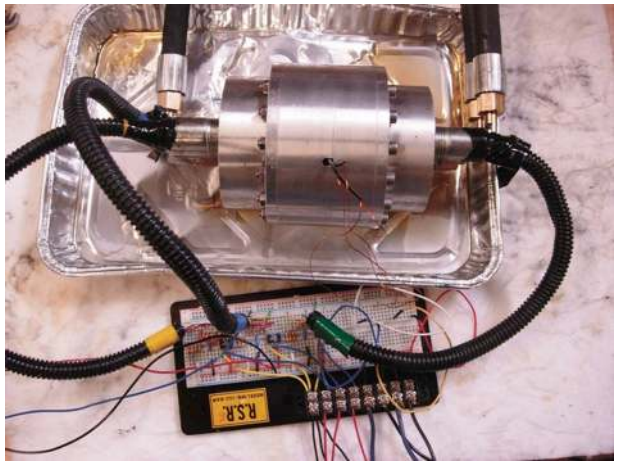

Fig. 12 Fluid test setup

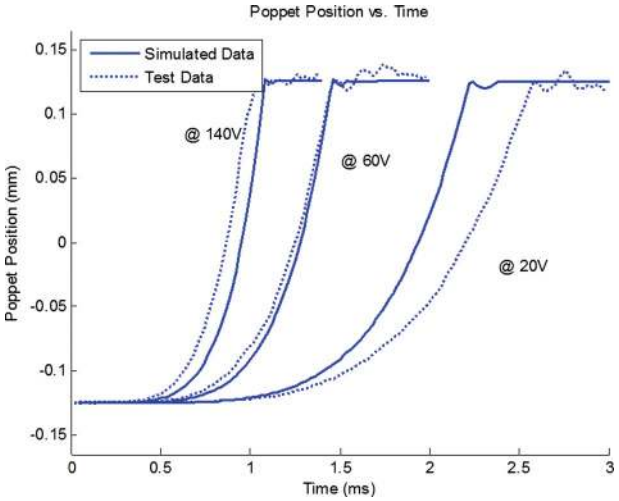

Fig. 13 Poppet transition profile at 140 V, 60 V, and 20 V

testing was done at 60 V and 0.2 mm stroke with a 50% duty cycle. The flow was approximately 24 L/min. To eliminate the effect of electrical interference, the data was post processed using a fifth order Butterworth filter with a 2 kHz cutoff frequency and zero phase lag. The model captures transients in fluid very well. Differences result from effects of fluid inertia and turbulent pressure drops in the rest of the systems.

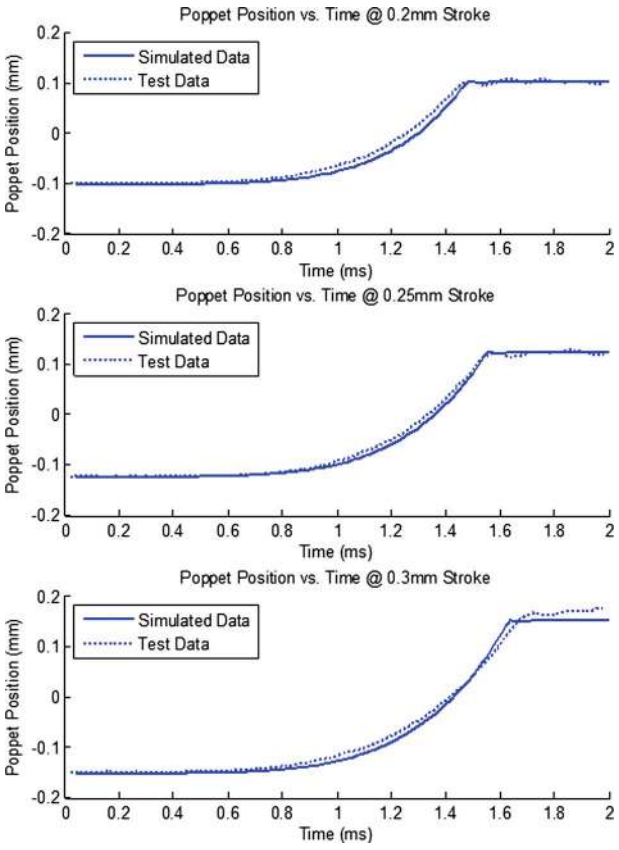

Fig. 14 Poppet transition profile at 0.20 mm, 0.25 mm, and 0.30 mm strokes

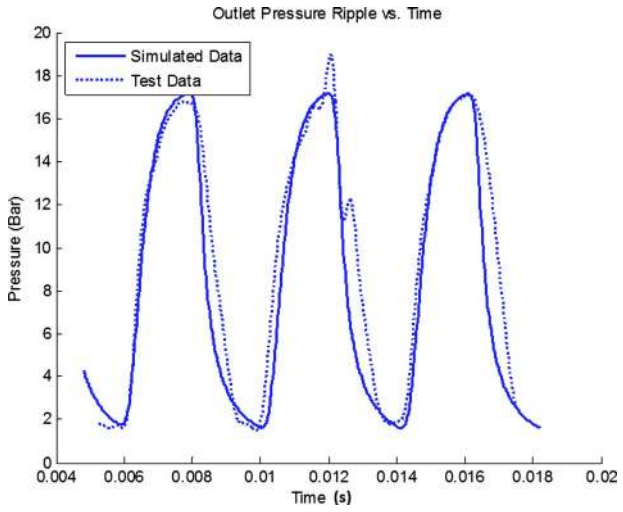

Fig. 15 Outlet pressure profile at 24LPM

8 Conclusions

A model was developed that accurately captures nonlinearities in the electromagnetic and fluidic domains. The forces in these two domains were then coupled to a mechanical domain to develop an overall model for a high speed on/off valve. A prototype with integrated sensors was manufactured to test the model. Model performance evaluation was done through both dry testing using a laser noncontact position measurement system, and fluid testing using high speed piezoresistive pressure transducers.

Acknowledgment

This work was funded through the National Science Foundation Center for Compact and Efficient Fluid Power under Grant No. EEC-0540834.

Nomenclature

A = cross sectional area (m^2)
b_{press} = pressure damping coefficient (m^2)
b_{valve_v0} = velocity damping coefficient (N s/m)
b_{wall} = wall damping coefficient (N s/m^2)
C_D = discharge coefficient
C_{DL} = laminar discharge coefficient
D_H = hydraulic diameter (m)
d = diameter (m)
E = bulk modulus (Pa)
F_{emag} = electromagnet force (N)
F_{Flow} = flow force (N)
F_{Fric} = friction force (N)
F_{total} = total force (N)
F_{wallb} = wall dampening force (N)
F_{wallK} = wall spring force (N)
g = air gap distance (m)
h = thickness (m)
i = coil current (A)
k_{wall} = spring constant (N/m)
$k_{leakage}$ = leakage coefficient (L/Pa)
K_q = flow gain (m^2/s)
K_c = pressure flow gain (L/Pa s)
K_{fq} = flow force gain (N/m)
K_{fc} = pressure flow force gain (m^2)
l_{valve} = poppet sealing length (m)
L = inductance (H)
m = mass (kg)
N = number of coil turns
P = permeability (Wb/A)
p = pressure (Pa)
Q = flow rate (L/min)
r = radial dimension (m)
r_{ref} = reference radius (m)
R = reluctance (A/Wb)
Re = Reynolds number
w = axial dimension (m)
state = control state
S = wetted perimeter (m)
t = time (s)
x = spool position (m)
Δx_{max} = valve stroke (m)
V_{comp} = compressed volume (L)
V_{decay} = decay voltage (V)
V_{in} = source voltage (V)
V_{line} = uncompressed line volume (L)
V_{sys} = system voltage (V)
β = valve coefficient (m/s)
θ = valve angle (rad)
μ = absolute permeability (H/m)
μ_0 = permeability of free space (H/m)
μ_{fl} = dynamic viscosity (Pa s)
μ_R = relative permeability
υ = kinematic viscosity (m^2/s)
ρ = fluid density (kg/m^3)
Ω = resistance (Ω)
σ = conductivity (S/m)
τ = time constant (s)
ϕ = magnetic flux (Wb)
ϕ_{inst} = instantaneous magnetic flux (Wb)

References

[1] Batdorff, M., and Lumkes, J., 2006, "Virtually Variable Displacement Hydraulic Pump Including Compressibility and Switching Losses," ASME Paper No. IMECE2006-14838.
[2] Shenouda, A., 2006, "Quasi-Static Hydraulic Control Systems and Energy Saving Potential Using Independent Metering Four-Valve Assembly Configuration," Ph.D. thesis, Georgia Institute of Technology, Atlanta, GA.
[3] Song, L., and Yao, B., 2002, "Energy-Saving Control of Single-Rod Hydraulic Cylinders with Programmable Valves and Improved Working Mode Selection," Proceedings of the 49th National Conference on Fluid Power (NCFP), National Fluid Power Association and Society of Automotive Engineers, Paper Nos. NCFP 102-2.4 and SAE OH 202-01-1343, pp. 81–90.
[4] Hu, H., Zhang, Q., and Alleyne, A., 2001, "Multi-Function Realization of a Generic Programmable E/H Valve Using Flexible Control Logic," *Proceedings of the Fifth International Conference on Fluid Power Transmission and Control*, International Academic Publishers, Beijing, China, pp. 107–110.
[5] Elfving, M., and Palmberg, J. O., 1997, "Distributed Control of Fluid Power Actuators-Experimental Verification of a Decoupled Chamber Pressure Controlled Cylinder," Proceedings of the Fourth International Conference on Fluid Power.
[6] Jansson, A., and Palmberg, J.-O., 1990, "Separate Control of Meter-In and Meter-Out Orifices in Mobile Hydraulic Systems," SAE Technical Paper No. 901583.
[7] Andruch, J., and Lumkes, J., 2008, "A Hydraulic System Topography With Integrated Energy Recovery and Reconfigurable Flow Paths Using High Speed Valves," Proceedings of the 51st National Conference on Fluid Power (NCFP), Paper No. NCFP I08-24.1, pp. 649–657.
[8] Merritt, H., 1967, *Hydraulic Control Systems*, Wiley, New York.
[9] Manring, N., 2005, *Hydraulic Control Systems*, Wiley, Hoboken, NJ.
[10] Lumkes, J., 2002, *Control Strategies for Dynamic Systems*, Dekker, New York.
[11] 1999, N-channel TrenchMOS™ Transistor, Phillips Electronics, NV, http://www.nxp.com/acrobat_download/datasheets/IRF640_S_1.pdf
[12] Pohl, J., Sethson, M., Krus, P., and Palmberg, J. O., 2002, "Modeling and Validation of a Fast Switching Valve Intended for Combustion Engine Valve Trains," Proc. Inst. Mech. Eng., Part I: J Systems and Control Engineering, **216**, pp. 105–116.
[13] Roters, H. C., 1941, *Electromagnetic Devices*, Wiley, New York.
[14] Karidis, J. P., 1983, "Modeling and Optimization of Fast-Acting Electromagnetic Actuators," Ph.D. thesis, Pennsylvania State University, State College, PA.

[15] Balakrishnan, A., Joines, W. T., and Wilson, T. G., 1997, "Air-Gap Reluctance and Inductance Calculations for Magnetic Circuits Using a Schwarz-Christoffel Transformation," IEEE Trans. Power Electron., **12**(4), pp. 654–663.
[16] Brauer, J. R., 2007, "Magnetic Diffusion Times for Infusion and Effusion in Nonlinear Steel Slabs and Cylinders," IEEE Trans. Magn., **43**(7), pp. 3181–3188.
[17] Ivantsyn, J., and Ivantysynova, M., 2003, *Hydrostatic Pumps and Motors*, 1st ed., Tech Books International, New Delhi, India.
[18] Meriam, J. L., and Kraige, L. G., 2002, *Engineering Mechanics*, 5th ed., Wiley, Hoboken, New Jersey, Vol. 2.
[19] 2006, CCD Laser Displacement Sensor, General Catalog, LK-G Series, Keyence Corp., Woodcliff Lake, NJ, http://www.keyence.com/products/vision/laser/lkg/lkg.php